IEEE Access
Multidisciplinary ⋮ Rapid Review ⋮ Open Access Journal

Received 16 May 2024, accepted 3 July 2024, date of publication 10 July 2024, date of current version 18 July 2024.

Digital Object Identifier 10.1109/ACCESS.2024.3426357

RESEARCH ARTICLE

DC-Sync: A Doppler-Compensation Time-Synchronization Scheme for Complex Mobile Underwater Sensor Networks

SUN DAJUN, OUYANG YUJIE, AND HAN YUNFENG

National Key Laboratory of Underwater Acoustic Technology, Harbin Engineering University, Harbin 150001, China
Key Laboratory of Marine Information Acquisition and Security (Harbin Engineering University), Ministry of Industry and Information Technology, Harbin 150001, China
College of Underwater Acoustic Engineering, Harbin Engineering University, Harbin 150001, China

Corresponding author: Han Yunfeng (hanyunfeng@hrbeu.edu.cn)

This work was supported by the National Key R&D Program of China, Grant No: 2021YFC 2801300, An AUV Research and Validation;
This work was supported by the Taishan Scholars Program.

ABSTRACT Time synchronization is crucial for effective collaboration among underwater sensors. However, existing synchronization protocols primarily cater to low-speed or simple motion scenarios, neglecting variations in radial velocity during message propagation. A novel Doppler compensation time synchronization scheme, called DC-Sync, was developed in this study to address this issue by targeting complex moving underwater sensors. DC-Sync includes a practical Doppler compensation and estimation method. Simulation results demonstrate that when the target motion follows a specific pattern, DC-Sync outperforms existing similar schemes in terms of time skew and time offset accuracy. Furthermore, the scheme maintains high estimation accuracy even with incomplete Doppler measurement values. Its performance was also validated through physical experiments.

INDEX TERMS Underwater timing, time synchronization protocol, Doppler estimates, clock skew and offset estimation.

I. INTRODUCTION

A unified time frequency primary standard is crucial for underwater sensor networks. When employed as an observation node, a globally unified timestamp is required; when serving as a navigation reference node, a high-precision synchronous clock can facilitate precise one-way-travel time (OWTT) navigation. Similar to the global positioning system's inability to provide absolute clocks, there is no ''absolute'' clock underwater. Thus, underwater time synchronization protocols have become indispensable. However, due to the unique characteristics of underwater acoustic communication networks, such protocols face challenges such as high signal propagation delay and time-varying propagation delay.

The associate editor coordinating the review of this manuscript and approving it for publication was Yougan Chen.

In response to the high propagation delay of underwater signals, [1] proposed time synchronization for high latency acoustic networks (TSHL), which performs hybrid synchronization based on one-way-travel and two-way-travel. However, TSHL assumes a constant propagation delay between sensor nodes, rendering it suitable only for static networks and generally inapplicable for mobile nodes affected by ocean currents or underwater vehicles with autonomous mobility capabilities.

The MU-Sync algorithm, a time synchronization protocol for underwater mobile networks, was proposed in [2] for the time-varying delay caused by underwater node movement. My-Sync achieves synchronization through multiple two-way-travel information exchanges, however, it assumes that the one-way propagation delay is half of the round-trip time. This can cause significant errors when nodes move quickly or when the response time of the nodes to-be-synchronized is prolonged.

References [3], [4], and [5] predicted the movement speed of synchronous nodes based on their mobility and spatial correlation. However, in practice, it is difficult to determine the exact correlation between adjacent nodes, especially when there is substantial distance between nodes.

The radial movement between nodes causes a Doppler frequency shift in the signals. Based on this, [6] designed an algorithm for Doppler-based time synchronization for mobile underwater sensor networks, called D-Sync, which functions based on physical layer information. D-Sync adopts two-way-travel message exchange synchronization, where the radial distance between nodes is calculated based on estimated Doppler frequency shifts. Under the assumption of a constant speed of sound, the two-way propagation delay is compensated to obtain the one-way propagation delay, achieving time synchronization. However, D-Sync does not consider the impact of clock skew in estimating the Doppler scaling factor; its timing accuracy decreases as the initial clock skew increases.

To further improve the accuracy of Doppler frequency shift estimation, [7] proposed a Doppler-assisted time synchronization scheme for mobile underwater sensor networks, the DA-Sync algorithm. When estimating the Doppler scale factor, DA-Sync not only considers node mobility but also the impact of clock skew. The radial speed is calculated from the estimated Doppler frequency shift, then a Kalman filter is used to refine the speed, which compensates for estimation errors caused by clock skew. However, DA-Sync assumes that the radial velocity between the reference node and the node to-be-synchronized varies linearly, which is not realistic as far as actual underwater environments and to some extent limits the accuracy of time synchronization.

Reference [8] proposed an algorithm for Doppler-enhanced time synchronization of mobile underwater sensor networks, DE-Sync, which accounts for both node mobility and the influence of clock skew while replacing the radial velocity between nodes with the Doppler scale factor. It is also the main comparison schemes in this article. Compared to DA-Sync, DE-Sync simplifies the linear regression process and achieves higher computational efficiency. It further improves time synchronization accuracy as it does not involve sound speed calculations. Similar to the DA-Sync algorithm, DE-Sync replaces radial velocity with the Doppler factor under the assumption that the radial velocity between nodes varies linearly, disregarding velocity changes between one-way-travel message exchanges.

Reference [9] proposed an adaptive power-efficient time synchronization for mobile underwater sensor networks called the APE-Sync algorithm. APE-Sync enhances the efficiency of subsequent long-term synchronization after DE-Sync by requiring only one message exchange for resynchronization. However, it does not fundamentally compensate for the simplified error caused by node motion.

The primary objective of underwater time synchronization algorithms is to solve the problem of long-time dynamic propagation delay estimation in underwater node networks, particularly the time-varying propagation delay caused by inter-node movement, which is the primary design target of existing methods. Through analysis of existing protocols, a Doppler-compensated underwater sensor time synchronization scheme, called DC-Sync, was developed in the present study. The closest protocol to this scheme is DE-Sync, with several key differences between them. Firstly, DC-Sync takes into account the difference caused by the movement of the wave source and receiver when correcting the Doppler scaling factor caused by clock skew, yielding more realistic results. Secondly, DC-Sync uses an equivalent value instead of an average value when estimating the Doppler scale factor, achieving higher synchronization accuracy and efficiency when dealing with nodes moving nonlinearly. Thirdly, DC-Sync accounts for the overall motion state of nodes during the interaction period to correct and compensate for all Doppler observations. This method remains applicable even when Doppler observations are missing for one of the one-way-travel message exchanges. A performance comparison between DC-Sync and DE-Sync was conducted for experimental verification purposes, as discussed in detail in the third and fourth sections of this paper.

II. METHODOLOGY

A. CLOCK MODEL OF TIME SYNCHRONIZATION PROTOCOL

As a prevalent time source for underwater time reference, the timing error of crystal oscillators can generally be attributed to two crucial technical indicators: long-term frequency stability and short-term frequency stability.

(1) Long-term stability refers to a change in frequency accuracy or drift rate over a considerable time span (generally days, weeks, months, years, or even longer), influenced by factors such as aging and temperature. Therefore, long-term stability can often be predicted.

(2) Short-term stability denotes the phase fluctuations or frequency fluctuations of the frequency source output signal within a timescale ranging from milliseconds to several hundred seconds, also known as ''second-level stability''.

The offset in a clock system is mainly attributable to the long-term frequency drift of the crystal oscillator, which accumulates over time. Thus, the essence of clock error is the long-term frequency stability of the crystal oscillator.

Long-term frequency stability refers to the directional drift rate of frequency over time, also referred to simply as ''aging''. The frequency aging of crystal oscillators can be positive or negative. The curve in Figure 1 illustrates the simplest aging model, where at least two frequency aging factors coexist as the crystal oscillator's frequency drift progresses over time.

The timekeeping process is radially short, so the frequency offset caused by aging of the crystal oscillator can be neglected. It is further assumed that clock offset does not accumulate during the timekeeping process, though clock skew and accumulated clock offset do exist before the timekeeping process begins.

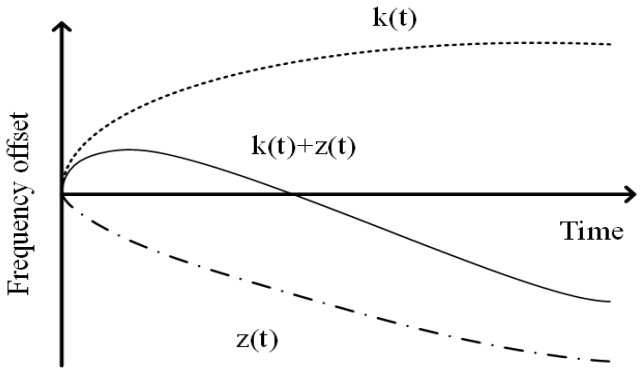

FIGURE 1. Frequency aging-time curve. The frequency drift of a crystal oscillator is not a perfectly linear phenomenon over a long period of time, such as several days or more. However, for short-term synchronization purposes, it is often reasonable to assume that the drift is linear within that short interval.

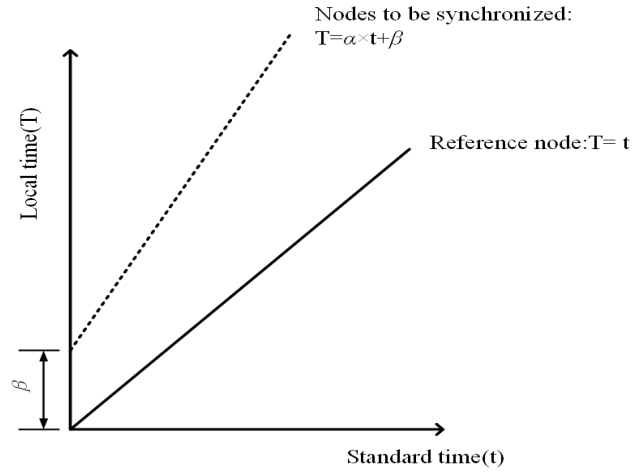

FIGURE 2. Linear clock error model. This is a general clock drift model that includes most time synchronization protocols such as MU-Sync, D-Sync, DA-Sync, and DE-Sync.

Assuming that the short-term frequency stability is a zero-mean random process, the clock skew occurring during the time synchronization process can be simplified as a constant. This results in a linear relationship between the system offset time axis and the standard time axis.

Based on these assumptions, we introduce the clock skew α, which represents the proportion of timing rhythm dislocation caused by the existing long-term frequency drift and short-term frequency fluctuations during the timekeeping process. We also introduce the clock offset β representing the timing error accumulated before the timekeeping process.

With this, we can now establish a mathematical model for clock error:

$$T = \alpha \times t + \beta \tag{1}$$

In (1), T represents the local time axis; t represents the standard reference time axis; α represents the clock skew; and β represents the clock offset. This model is also commonly used in other synchronization protocols [11], Such as MU-Sync [2], D-Sync [6], DA-Sync [7], DE-Sync [8], and so on. The DC-Sync time synchronization process consists of four stages: data collection, Doppler compensation, linear regression, and calibration. In the first stage, the node to-be-synchronized collects timestamps and Doppler scale factors through multiple bidirectional information exchanges. In the second stage, the impact of clock skew on Doppler observations is eliminated, followed by estimation of the overall motion state of the node to-be-synchronized to rectify the Doppler scale factors. In the third stage, the node to-be-synchronized uses the least squares estimation for an initial linear regression, thereby deriving the clock skew and offset. In the final stage, the initial clock skew value used in the second stage is updated, the Doppler scale factors are re-compensated, and another linear regression is performed. All relevant parameters are outlined in Table 1.

TABLE 1. Parameter comparison.

parameter	illustrate
A	Reference node
B	Nodes to be synchronized
α	Clock skew
β	Clock offset
$t_1[k]/t_4[k]$	Kth exchange, reference node send/receive timestamp
$T_2[k]/T_3[k]$	Kth exchange, nodes to be synchronized send/receive timestamp
$t_2[k]/t_3[k]$	Standard reference time corresponding to $T_2[k]/T_3[k]$
T_r	Response interval of nodes to be synchronized
a	Dopp scale factor caused by node movement
a_e	Equivalent values of Doppler scale factors between t_2 and t_4
v	radial velocity between nodes
c	Speed of sound
a_{AB}	Doppler scale factor measured by node **B**
a_{BA}	Doppler scale factor measured by node **A**
τ_1	Propagation delay from node **A** to **B**
τ_2	Propagation delay from node**B** to **A**
Δd	radial movement distance between t_2 and t_4

B. DATA COLLECTION

In DC-Sync, the synchronization request is initiated by node **A**. When node **A** detects that node **B** has moved into the network coverage area, it sends a synchronization request to **B** and records the sending time t_1. Upon receiving the request, node **B** records its local receiving time as T_2 and simultaneously records the measured Doppler scale factor a_{AB}. After an interval of time T_r, at the moment T_3, node **B** sends the timestamp information (T_2, T_3) and Doppler information a_{AB} back to node **A** in package form. Similarly, node **A** records the receiving time t_4 and measured Doppler scale factor a_{BA}. After several rounds of message exchanges, node **A** collects k sets of information $\{t_1[k], T_2[k], T_3[k], t_4[k], a^k_{\mathrm{AB}}, a^k_{\mathrm{BA}}\}$. The synchronization information exchange process is depicted in Figure 3.

C. DOPPLER COMPENSATION

Node **A** is a reference node with a standard time, and node **B** is a node to-be-synchronized with timing errors (skew α and offset β). The message with waveform $x_{AB}(t)$ is sent from node **A** and received at node **B** with waveform [12], [13]. The direction away from node **A** is considered positive, with a

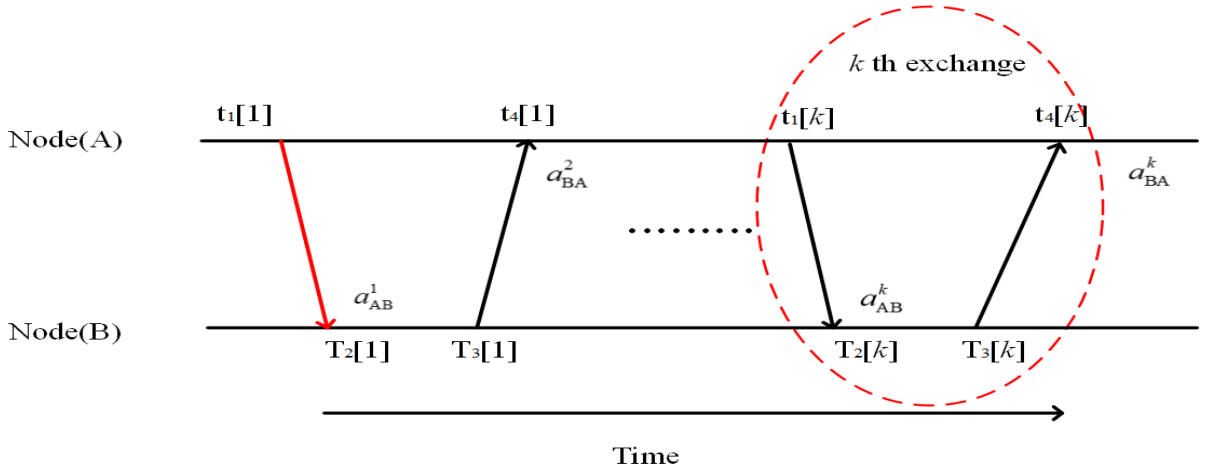

FIGURE 3. Message exchange process. Message exchange process. The initiator of message exchange is not necessarily the reference node, and can be changed according to the application scenario, platform capabilities and task requirements.

velocity of v. At this moment, the receiver moves away from the wave source:

$$y_{\mathrm{AB}}(t) = \sum_{p=1}^{N_p} A_p x_{AB}\left(\left(\frac{c-v}{c}\right)t - \tau_p\right) = \sum_{p=1}^{N_p} A_p x_{AB}\left((1-a)t - \tau_p\right) \quad (2)$$

In (2), $N_p$represents the number of paths while A_p and τ_p represent the amplitude and delay of the -th path, respectively. The received signal is discretized into $y_{AB}[n]$ according to f_s the sampling rate of node **A**. However, due to the clock skew of node **B**, the actual sampling rate is αf_s; the actual discretized samples of $y_{AB}(t)$ are:

$$y_{\mathrm{AB}}[n] = y_{\mathrm{AB}}(t)|_{t=n/\alpha f_s} = \sum_{p=1}^{N_p} A_p x_{AB}[\underbrace{\frac{(1-a)}{\alpha}}_{=1-a_{\mathrm{AB}}} \cdot \frac{n}{f_s} - \tau_p] \quad (3)$$

Similarly, the signal received by node **A** from node **B** can be obtained, where the mover is the wave source with a velocity of v.

$$y_{\mathrm{BA}}(T) = \sum_{p=1}^{N_p} A_p x_{\mathrm{BA}}\left(\left(\frac{c}{c+v}\right)T - \tau_p\right) = \sum_{p=1}^{N_p} A_p x_{\mathrm{BA}}\left(\left(\frac{1}{1+\alpha}\right)T - \tau_p\right) \quad (4)$$

The received signal is discretized $y_{BA}[n]$ according to the sampling rate f_s of node **A**, and $T = \alpha t$:

$$y_{\mathrm{BA}}[n] = y_{\mathrm{BA}}(T)|_{T=\alpha n/f_s} = \sum_{p=1}^{N_p} A_p x_{\mathrm{BA}}[\underbrace{\left(\frac{1}{1+a}\right)\alpha}_{=1/(1+a_{\mathrm{BA}})} \cdot \frac{n}{f_s} - \tau_p] \quad (5)$$

In (3) and (5):

$$a_{\mathrm{AB}} = \frac{L_{\mathrm{B}} - L_{\mathrm{ref}}}{L_B}, a_{\mathrm{BA}} = \frac{L_{\mathrm{A}} - L_{\mathrm{ref}}}{L_{\mathrm{ref}}} \quad (6)$$

where L_{A},L_{B}, and L_{ref} are the lengths of the received signal at node **A**, the received signal at node **B**, and the reference signal, respectively.

Based on the Doppler scale factor, the radial velocity between the two nodes at moments $t_2$andt_4 can be obtained as follows:

$$v\,(t_2) = a\,(t_2)\cdot c = (1-(1-a_{AB})\,\alpha)\,c \ \mathrm{A} \to \mathrm{B} \quad (7)$$

$$v\,(t_4) = a\,(t_4)\cdot c = ((1+a_{BA})\,\alpha - 1)\,c \ \mathrm{B} \to \mathrm{A} \quad (8)$$

It is important to note that the clock skew α in (6) is unknown during the first Doppler compensation and can only be obtained after the linear regression in the third stage is completed. Before this first iteration is completed, α is assigned an initial value of "1". The error introduced by this initial value is subsequently corrected during the calibration stage.

After all interactions are completed, k discrete radial velocity samples $v[n]|_{n=t_2[1],t_4[1],\cdots,t_2[\mathrm{k}],t_4[\mathrm{k}]}$ can be obtained.

let $v[n]|_{n=t_2[1],t_4[1],\cdots,t_2[\mathrm{k}],t_4[\mathrm{k}]} = v[n]|_{n=1,\cdots,2k}$

If either node **A** or node **B** cannot obtain Doppler information, the radial velocity samples $v[n]|_{n=t_2[1],\cdots,t_2[\mathrm{k}]}$ / $v[n]|_{n=t_4[1],\cdots,t_4[\mathrm{k}]} = v[n]|_{n=1,\cdots,k}$ can also be used.

$$f(x) = \boldsymbol{P}\begin{bmatrix} x^3 \\ x^2 \\ x^1 \\ 1 \end{bmatrix}, \varphi(\boldsymbol{P}) = \sum_{n=1}^{2k}(v(n) - f(n,\boldsymbol{P})) \quad (9)$$

When $\varphi(\boldsymbol{P}) = \min$, the radial velocity estimation curve $f(x)|_{x\in(t_2[1],t_4[\mathrm{k}]}$ for the entire synchronization stage can be obtained, alongside the corresponding Doppler scale factor curve $\lambda(x)|_{x\in(t_2[1]t_4[\mathrm{k}])} = f(x)/c$ for the entire synchronization stage.

D. LINEAR REGRESSION

Considering the round-trip process of synchronization messages and in conjunction with (1), the following holds:

$$T_2 = \alpha\left(t_1 + \tau_1\right) + \beta \tag{10}$$
$$T_3 = \alpha\left(t_4 - \tau_2\right) + \beta \tag{11}$$

By adding and subtracting the propagation delays τ_1 and τ_2, respectively, we can obtain:

$$\tau_2 + \tau_1 = \left(T_2 - T_3\right)/\alpha + t_4 - t_1 \tag{12}$$
$$\tau_2 - \tau_1 = \Delta d/c \tag{13}$$

where $\Delta d = \int_{t_2}^{t_4} f(x)dx = \mathrm{c} \cdot \int_{t_2}^{t_4} \lambda(x)dx$. The equivalent Doppler scale factor is $a_e\left(t_4 - t_2\right) = \int_{t_2}^{t_4} \lambda(x)dx$, which can be substituted it into (10) and (11) as follows:

$$\tau_2 - \tau_1 = a_e\left(t_4 - \left(T_2 - \beta\right)/\alpha\right) \tag{14}$$

Combining (10), (11), (12) and (13) allows us to solve for $\tau_1$and τ_2, respectively:

$$\tau_1 = \frac{\left(1 + a_e\right)T_2 - T_3 - a_e\beta}{2\alpha} + \frac{t_4\left(1 - a_e\right)}{2} - \frac{t_1}{2} \tag{15}$$
$$\tau_2 = \frac{\left(1 - a_e\right)T_2 - T_3 + a_e\beta}{2\alpha} + \frac{t_4\left(1 + a_e\right)}{2} - \frac{t_1}{2} \tag{16}$$

Substituting either τ_1 or τ_2 into (9) yields:

$$T_3 + \left(1 - a_e\right)T_2 = \left(t_4\left(1 - a_e\right) + t_1\right)\alpha + \left(2 - a_e\right)\beta \tag{17}$$

According to (15) and (16) linear regression can be employed to estimate skew α and offset β:

$$\hat{\mu} = \left[\hat{\alpha}\ \hat{\beta}\right]^{\mathrm{T}} = \left(\mathbf{H}^{\mathrm{T}}\mathbf{H}\right)^{-1}\mathbf{H}^{\mathrm{T}}\mathbf{Z} \tag{18}$$

$$\mathbf{H} = \begin{bmatrix} \left(t_4[1]\left(1 - a_e[1]\right) + t_1[1]\right) & \left(2 - a_e[1]\right) \\ \vdots & \vdots \\ \left(t_4[k]\left(1 - a_e[k]\right) + t_1[k]\right) & \left(2 - a_e[k]\right) \end{bmatrix},$$
$$\mathbf{Z} = \begin{bmatrix} T_3[1] + \left(1 - a_e[1]\right)T_2[1] \\ \vdots \\ T_3[k] + \left(1 - a_e[k]\right)T_2[k] \end{bmatrix} \tag{19}$$

In (19), $a_e[k]$ is the equivalent value of the Doppler scale factor in the kth interaction; $\hat{\alpha}$ and $\hat{\beta}$ are the estimated values of the true skew and offset, respectively.

E. CALIBRATION

In the second stage of Doppler compensation, the clock skew is assigned an initial value of "1", which obviously needs to be corrected. In the calibration stage, DC-Sync uses the estimated skew $\hat{\alpha}$ to update the initial skew value and perform Doppler compensation and linear regression estimation again. The calibration process iterates until the termination conditions are met, e.g., the number of iterations exceeds 5 or the difference between adjacent clock skew estimates falls below 10 ppm.

III. TIME SYNCHRONIZATION ERROR ANALYSIS

A. THE IMPACT OF TIME DELAY ESTIMATION ERRORS

In the process of time synchronization, the receiver is considered as a passive system, and the received signal is composed of the target signal and noise. Assuming that the target signal and noise are uncorrelated and are stationary random processes, the Cramér-Rao lower bound (CRLB) [14] of the delay estimate using the coherence function radial to the true value is:

$$\varepsilon_\tau \geq \left\{2T\int_0^\infty (2\pi f)^2 \frac{|\gamma(f)|^2}{\left[1 - |\gamma(f)|^2\right]}df\right\}^{-1} \tag{20}$$

where, ε_τ is the variance of the time delay estimation near the true time delay, $\gamma(f)$ is the coherence function, and T is the observation time. ↓ When SNR $\ll 1$, the standard deviation of the delay estimation was:

$$\varepsilon_\tau \geq \left(\frac{3}{8\pi^2 T}\right)^{\frac{1}{2}} \frac{1}{\mathrm{SNR}} \frac{1}{\sqrt{f_2^3 - f_1^3}} \tag{21}$$

When SNR $\gg 1$,

$$\varepsilon_\tau \geq \left(\frac{3}{4\pi^2 T}\right)^{\frac{1}{2}} \frac{1}{\sqrt{\mathrm{SNR}}} \frac{1}{\sqrt{f_2^3 - f_1^3}} \tag{22}$$

From the second section, we can see that the main input parameters of the time synchronization algorithm between platforms are timestamp information and Doppler scale factor, and the time delay estimation error will directly affect the accuracy of timestamp information. And the two are consistent in size, that is, the timestamp information error is $\varepsilon_T = \varepsilon_\tau$.

The linear regression equation of DC Sync synchronization method is shown in (17), and by adding timestamp information error, it can be obtained:

$$T_3 + \left(1 - a_e\right)T_2 = \left(t_4\left(1 - a_e\right) + t_1\right)\alpha + \left(2 - a_e\right)\beta + \varepsilon \tag{23}$$

The results are as follows:

$$T_3 + \left(1 - a_e\right)T_2 = \left(t_4\left(1 - a_e\right) + t_1\right)\left(1 + \frac{\left(2 - a_e\right)\varepsilon_T}{t_4\left(1 - a_e\right) + t_1}\right)\alpha + \left(2 - a_e\right)\left(\beta + \varepsilon_T\right) \tag{24}$$

Let $\hat{\alpha} = \left(1 + \frac{(2-a_e)\varepsilon_T}{t_4(1-a_e)+t_1}\right)\alpha$, $\hat{\beta} = \beta + \varepsilon_T$, then:

$$\varepsilon_{\alpha_{\mathrm{DC}}} = \hat{\alpha} - \alpha = \frac{\left(2 - a_e\right)\varepsilon_T}{t_4\left(1 - a_e\right) + t_1}\alpha$$
$$\varepsilon_{\beta_{\mathrm{DC}}} = \hat{\beta} - \beta = \varepsilon_T \tag{25}$$

In general $a_e \ll 1$, $\alpha \approx 1$, (25) can be simplified as:

$$\varepsilon_{\alpha_{\mathrm{DC}}} \approx \frac{2\varepsilon_T}{t_1 + t_4} = \frac{\varepsilon_T}{t_1 + T_{delay}}$$
$$\varepsilon_{\beta_{\mathrm{DC}}} = \varepsilon_T \tag{26}$$

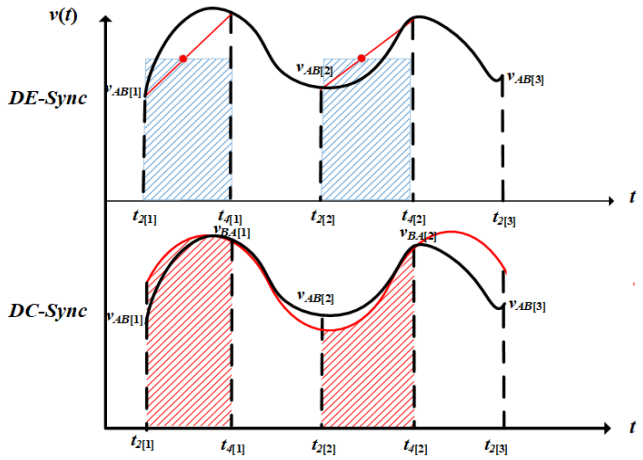

FIGURE 4. Comparison of DE-Sync protocol and DC-Sync protocol for radial motion velocity estimation.

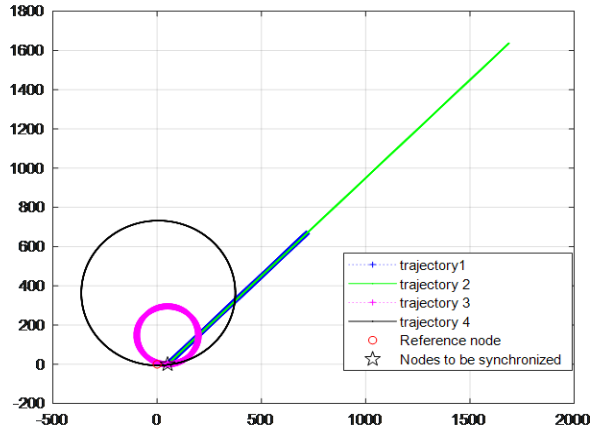

FIGURE 5. Simulated trajectories. The simulation designs four trajectories in the figure based on the trend and rate of radial velocity changes between nodes.

B. THE IMPACT OF DOPPLER ERROR

Unlike the DE algorithm, the DC algorithm considers the radial movement between nodes throughout the entire interaction process, and obtains more accurate and continuous Doppler interpolation by fitting the overall motion state, thereby better estimating the actual radial motion distance, as shown in Figure 4. This figure shows the comparison of the radial motion speed estimated by the DE-Sync method and the DC method. The black curve represents the change in radial motion speed between nodes; the area enclosed by the black curve and the horizontal axis represents the actual radial motion distance; the red dots represent the average value of the radial motion speed between the two receiving ends used in calculating the radial motion distance by the DE-Sync method in this article; the blue shaded area represents the radial motion distance between nodes calculated by the DE-Sync method in this article. The red curve $f(t)$ represents the radial motion speed curve estimated by the DC-Sync method in this article; the red shaded stripe represents the radial motion distance between nodes

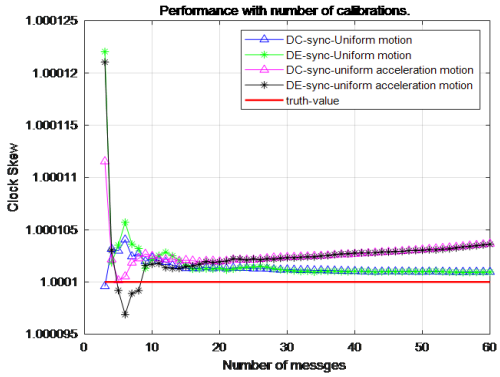

(a) Time skew

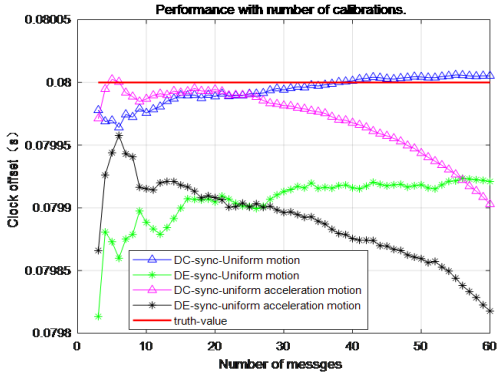

(b) Time offset

FIGURE 6. Comparison of DC-Sync and DE-Sync estimation accuracy for linear trajectories 1 and 2.

calculated by the DC-Sync method in this article. It can be seen that in non-uniform linear motion, the DC method has higher estimation accuracy.

$$\varepsilon_{\text{doppler}} = \int_{t_2}^{t_4} (f(t) - v(t))dt/c \tag{27}$$

Similarly, substituting the Doppler error $\varepsilon_{\text{dbppler 2}}$ into (17), we can obtain:

$$\begin{aligned} &T_3 + (1 - a_e)\, T_2 \\ &\quad = (t_4\,(1 - a_e) + t_1)\,\alpha + (2 - a_e)\,\beta + \varepsilon \end{aligned} \tag{28}$$

where $\varepsilon = \varepsilon_{\text{doppler}} \times (T_2 - \alpha t_4 - \beta)$, combining (28), (10) and (11):

$$\begin{aligned} \varepsilon &= \varepsilon_{\text{doppler}} \times (T_2 - T_3 - \tau_2) \\ &= -\varepsilon_{\text{doppler}} \times (T_r + \tau_2) \end{aligned} \tag{29}$$

where, T_r is the response interval of the node B to be synchronized. Substituting it into (18):

$$\begin{bmatrix} \varepsilon_{\alpha_{1C}} \\ \varepsilon_{\beta_{BC}} \end{bmatrix} = \left(\mathbf{H}^{\mathrm{T}}\mathbf{H}\right)^{-1} \mathbf{H}^{\mathrm{T}}\boldsymbol{\varepsilon} \tag{30}$$

where, $\boldsymbol{\varepsilon} = \begin{bmatrix} \varepsilon[1] \\ \vdots \\ \varepsilon[k] \end{bmatrix}$, $\varepsilon[k]$ is the linear equation error term caused by the platform's movement during the k th interaction. the synchronization error caused by movement is mainly reflected in the estimation of clock offset.

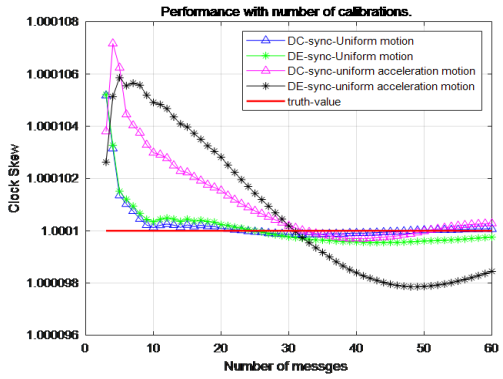

(a) Time skew

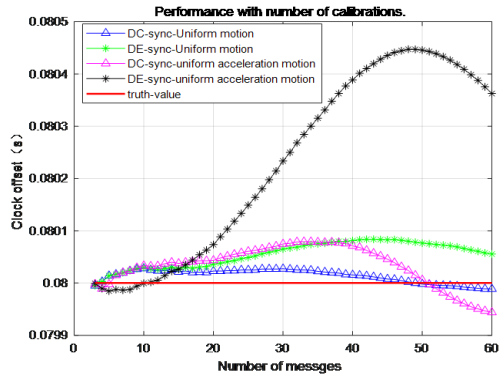

(b) Time offset

FIGURE 7. Comparison of DC-Sync and DE-Sync estimation accuracy for circular trajectores 1 and 2.

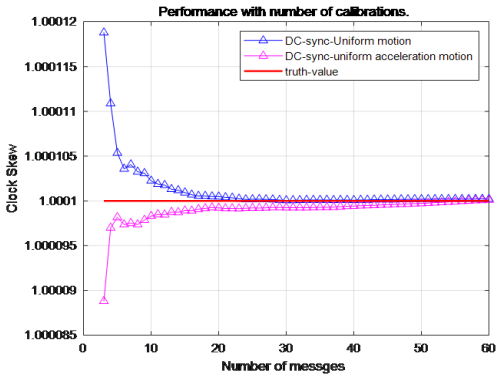

(a) Time skew

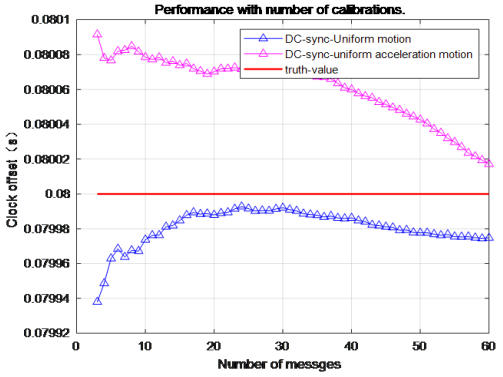

(b) Time offset

FIGURE 8. Synchronization Accuracy of the DC-Sync in the Absence of Doppler Information.

IV. PERFORMANCE EVALUATION

A. SIMULATION SETTINGS

The frequency stability of common active crystal oscillators is 100ppm, so the inherent clock skew of the node to-be-synchronized is 100ppm and the initial clock offset is 80 ms. The response delay T_r is 0.5 s (in the local clock scale), the interaction period is 4 s, and the maximum number of interactions is 60. The signal length is 200 ms. Considering a delay estimation error of 10μs, the Doppler measurement error is set to follow a normal distribution of $\mathrm{N} \sim \left(0, 5 \times 10^{-6}\right)$. The movement trajectories of the node to-be-synchronized were divided here into four types, as delineated in Figure 5.

The reference node coordinates are $(0, 0)$ and the coordinates of the node to-be-synchronized are $(50, 0)$. The node movement direction error is set to follow a normal distribution of $\mathrm{N} \sim \left(0, 2 \times 10^{-5}\pi\right)$. Various trajectory parameters were set considering that the experimental ship speed is generally lower than five knots, and the acceleration of a 400-ton unloaded cargo ship is generally lower than $0.012\ \mathrm{m/s^2}$. Track 1 has a movement speed of 2 m/s. Track 2 has an initial speed of 2 m/s and an acceleration of $0.012\ \mathrm{m/s^2}$; acceleration ceases when the speed increases to 5 m/s. Track 3 has a movement speed of 2 m/s and Track 4 has a movement speed of 5 m/s.

B. ANALYSIS OF SIMULATION RESULTS

1. Comparison of estimation accuracy under linear trajectory, where radial velocity changes are approximately linear

As discussed in this section, we evaluated the performance of DC-Sync and DE-Sync under the simulation conditions given in IV-A. In the scenarios of Track 1 and Track 2 given in IV-A, the results for DC and DE methods are provided in Figure 6.

Under this trajectory, the radial velocity between nodes changes almost linearly. At this time, DC-Sync and DE-Sync schemes both have radially high accuracy and gradually converge as the number of interactions increases, stabilizing after 20 iterations. Along Track 1, which has uniform linear motion, the estimation accuracy of DC and DE methods for clock skew are similar – both lower than 1×10^{-6}. The estimation accuracy of DC for clock offset is approximately 5μs and that of DE is about 75μs. On Track 2, which features uniform acceleration linear motion, the clock skew and offset estimation accuracies for both DC and DE methods gradually decline as the radial velocity increases. The clock skew of DC is consistent with DE, approximately 4×10^{-6}. The worst estimation accuracy of DC for clock offset is 100μs and the worst estimation accuracy of DE for clock offset is 180μs.

2. Comparison of estimation accuracy under circular trajectory, where radial velocity changes are nonlinear.

(a) Moving ordinary node **B**

(b) Stationary reference node **A**

FIGURE 9. Experimental platform. Node B travels on the lake surface according to a pre-designed trajectory and speed, simulating a moving node. Node A anchors itself to simulate a reference node.

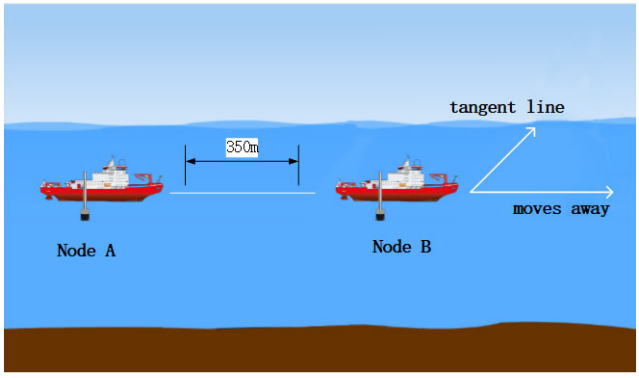

FIGURE 10. A schematic diagram of the time synchronization test scenario, which roughly shows the motion trajectory of ship B in the synchronization scenario and the simulated motion node.

When the movement trajectory of node **B** changes from 1 and 2 to 3 and 4, the radial movement velocity is no longer linear. This is a common situation encountered in engineering practice. In figure 7, as the movement speed of node **B** increases (from Track 3 to Track 4) and the synchronization accuracy of DC-Sync is significantly better than that of DE-Sync. The estimation accuracy of DC for clock skew remains below 3×10^{-7}, while that of DE for clock skew on Track 4 (high-speed state) is 2×10^{-6}. The worst estimation accuracy of the DC method for clock offset is 100μs, while that of DE is 450μs.

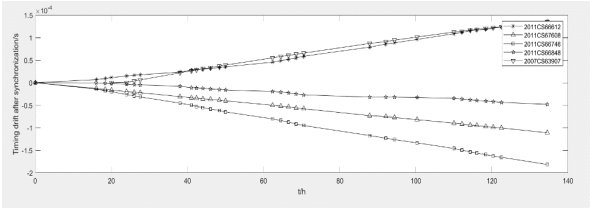

FIGURE 11. Cumulative timing error characteristic of *SA.45s* rubidium clock over 135 hour.

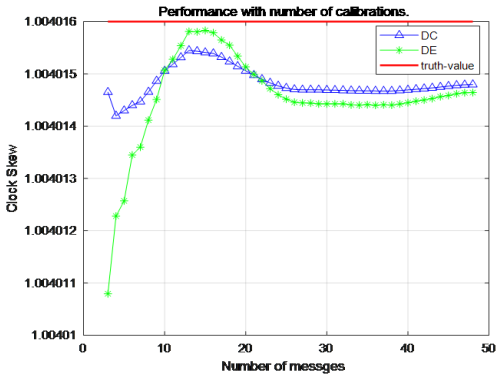

(a) Time skew

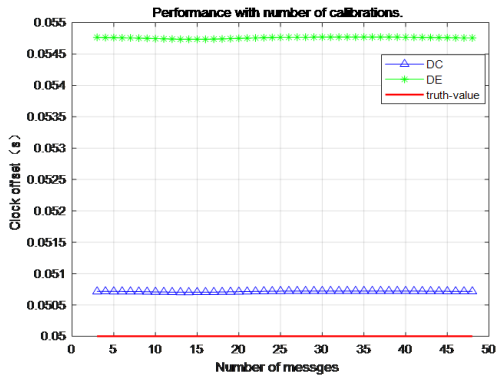

(b) Time offset

FIGURE 12. Performance comparison between DC-Sync and DE-Sync when two nodes are radially stationary and there is no change in radial velocity.

3. Synchronization accuracy analysis of DC method with incomplete doppler information on circular trajectories.

In figure 8, when node **B** cannot measure Doppler information, the DE method is no longer applicable. The estimation results of the DC method in this case are depicted in Figure 8. The estimation accuracy of DC-Sync for clock skew remains below 2×10^{-7}, while that for clock offset is below 100μs, with the highest value reaching 20μs.

In conclusion, during the time synchronization process of DC-Sync and DE-Sync schemes, larger overall radial velocity drives down estimation accuracy. When the radial acceleration changes are approximately linear, DC and DE methods show similar estimation accuracy for clock skew but the DC method's offset estimation accuracy is higher. When the radial acceleration changes nonlinearly, the estimation accuracy of the DC method is generally better than that of the

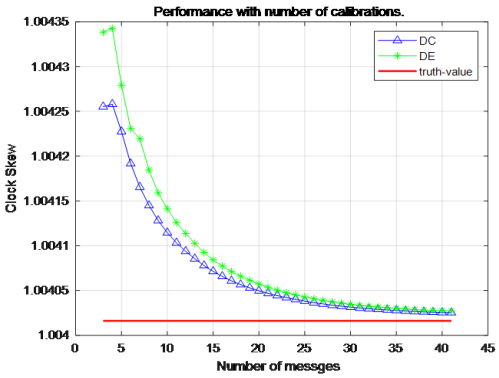

(a) Time skew

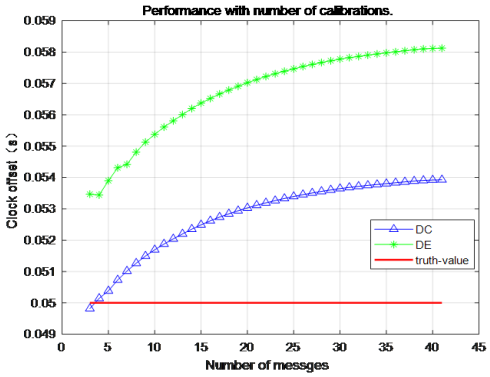

(b) Time offset

FIGURE 13. Performance comparison between DC-Sync and DE-Sync when the radial velocity changes approximately linearly as node B gradually moves away from node A.

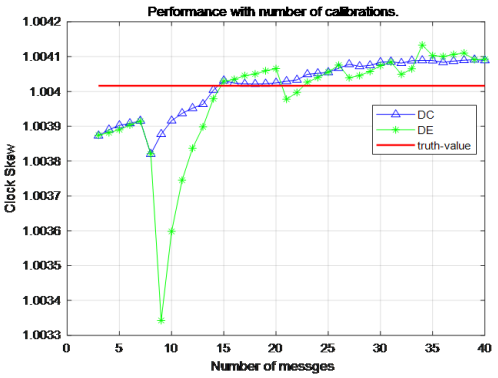

(a) Time skew

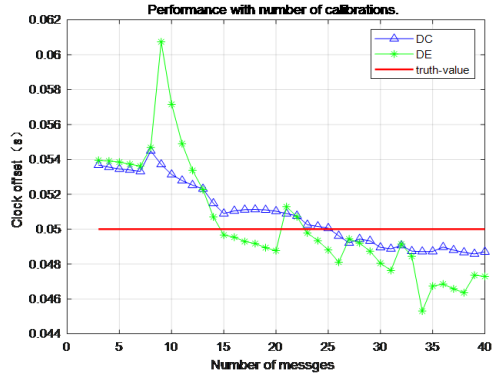

(b) Time offset

FIGURE 14. Performance comparison between DC-Sync and DE-Sync when Node B passes along the tangent line at a distance of 350 meters from Node A, and the radial velocity first decreases and then increases.

DE method; DE's accuracy decreases significantly as speed increases. When Doppler information is missing for node **B**, the DE method is not applicable but the DC method maintains radially high estimation accuracy. Therefore, the DC method outperforms the DE method overall. Its applicability is also markedly stronger in complex radial motion states or when Doppler information is partially missing.

V. VERIFICATION OF MEASURED DATA

A. EXPERIMENTAL OVERVIEW

On August 26, 2023, the time synchronization test was carried out in Danjiangkou, Henan Province. The participating ships are shown in the figure 9, and the test scene on the lake is shown in Figure 10. The communication signal frequency band is 8-16kHz. ship A achieves the timing of ship B through multiple information interactions on the preset timing trajectory with the assistance of the GNSS time reference. The ships simulate the reference node **A** and the synchronization node **B**, both using the atomic clock SA.45s as the external clock source for sampling and time stamp recording.

The CSAC rubidium clock, model SA.45s, has a cumulative drift over 135 hours as shown in Figure 11 which can be considered constant for short-term time synchronization. By adjusting the rubidium clock parameters, the actual clock skew α of node **B**'s clock source reached 1.004016 and the clock offset β was 50ms.

B. ANALYSIS OF EXPERIMENTAL RESULTS

Due to the inherent difficulty of controlling the direction of the experimental vessels, the experiment simulated different radial velocity changes through various linear trajectories.

In the first case, Node B drifts 350 meters away from node **A** while both are radially stationary. In figure 12, the clock skew estimation accuracy is better than 1×10^{-5}; the DC clock offset estimation accuracy surpasses 0.7ms and the DE method is better only than 4.8ms.

In the next case, Node B gradually moves away from node **A**, with radial velocity changing approximately linearly. In figure 13, the clock skew estimation accuracy is better than 4×10^{-5}. The DC clock offset estimation accuracy is better than 4ms and the DE method is only better than 8.2ms. In any interaction, the DC method outperforms the DE method.

Lastly, Node B passes node **A** in a straight line at a distance of 350 meters with radial velocity first decreasing and then increasing. In figure14, the highest clock skew estimation accuracy exceeds 7×10^{-5}, the DC clock offset estimation accuracy surpasses 4.6ms, and the DE method's maximum estimation error reaches 10.7ms.

In the scenario corresponding to Figure 15, without using Doppler information from node **B**, the estimation accuracy of

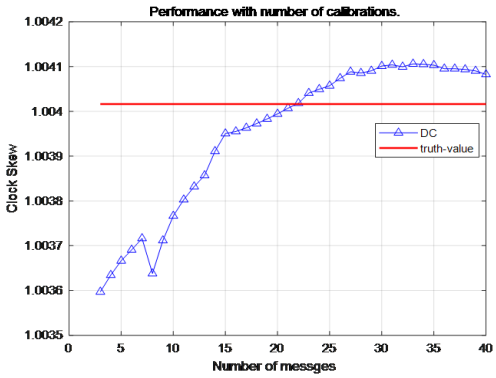

(a) Tkew

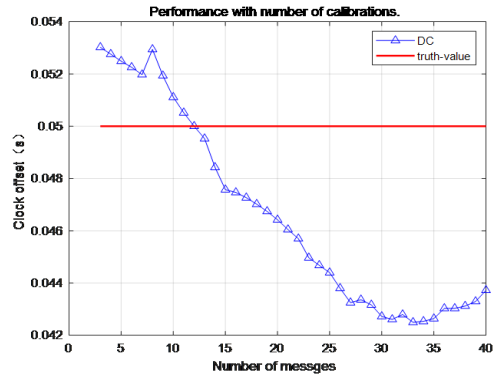

(b) Time offset

FIGURE 15. The synchronization accuracy of DC-Sync under incomplete Doppler measurement values.

the DC method decreases and clock skew estimation accuracy drops to 7.7×10^{-5}. The clock offset estimation accuracy is only better than 7.5*ms* in this case. ime sFurthermore, as evident in Figures 12 and 13, the DC method exhibits a more significant correction effect on Doppler estimation values when radial velocity is low, the Doppler changes linearly, and the estimation error accumulates gradually. However, when the radial velocity changes nonlinearly, the Doppler estimation errors throughout the entire motion process may cancel each other out, thereby reducing their impact. Regardless of whether the change is linear or nonlinear, the DC method outperforms the DE method in terms of clock skew and offset estimation accuracy. It also retains its radially high estimation accuracy in cases when some Doppler information is missing.

VI. CONCLUSION

This paper introduces a synchronization scheme called DC-Sync, which is designed specifically to address nonlinear movement within underwater sensor networks. DC-Sync operates as a Doppler compensation-based time synchronization scheme. By evaluating the overall motion state of mobile nodes, DC-Sync recalibrates Doppler measurements during the message exchange period and thereby enhances the accuracy of Doppler scale factor estimations. DC-Sync also employs the Doppler equivalent value instead of the average value to estimate propagation delay, which improves delay estimation accuracy. /par Simulation results show that when nodes have linear motion, the proposed Doppler compensation approach significantly improves the accuracy of time offset estimation compared to other methods. Even in cases of complex node motion and missing Doppler measurements, it effectively improves synchronization accuracy and maintains high-quality estimation capability. Lake test results demonstrated that under linear motion, the clock offset estimation accuracy of DC-Sync improves by 4*ms* compared to the DE-Sync algorithm. The overall accuracy is higher under nonlinear motion. When the Doppler information for non-reference nodes is missing, DC-Sync yields clock offset accuracy still higher than 7.5*ms*. /par In the future, we plan to further validate the DC-Sync scheme on a sea trial platform and further explore its performance under more complex motion conditions.

REFERENCES

[1] A. Syed and J. Heidemann, "Time synchronization for high latency acoustic networks," presented at the 25th IEEE Int. Conf. Comput. Commun., Joint Conf. IEEE Comput. Commun. Societiess, Apr. 2006.

[2] N. Chirdchoo, W. Soh, and K. Chua, "MU-Sync: A time synchronization protocol for underwater mobile networks," presented at the 3rd Workshop Underwater Netw., Sep. 2008, doi: 10.1145/1410107.1410115.

[3] Y. Dong, R. Wang, Z. Li, Z. Li, K. Zhang, and Y. Zhai, "A novel time synchronization algorithm for underwater wireless sensor networks with mobility prediction," in *Proc. 3rd IEEE Int. Conf. Comput. Commun. (ICCC)*, Dec. 2017, pp. 373–377, doi: 10.1109/COMPCOMM.2017.8322574.

[4] G. Liu, J. Tian, and W. Kong, "An iterative algorithm for clock synchronization of underwater sensors based on node velocimetry," *Comput. Eng. Design*, vol. 41, no. 6, p. 6, 2020.

[5] J. Liu, Z. Zhou, Z. Peng, J.-H. Cui, M. Zuba, and L. Fiondella, "Mobi-sync: Efficient time synchronization for mobile underwater sensor networks," *IEEE Trans. Parallel Distrib. Syst.*, vol. 24, no. 2, pp. 406–416, Feb. 2013, doi: 10.1109/TPDS.2012.71.

[6] F. Lu, D. Mirza, and C. Schurgers, "D-sync: Doppler-based time synchronization for mobile underwater sensor networks," presented at the 5th Int. Workshop Underwater Netw., Sep. 2010, doi: 10.1145/1868812.1868815.

[7] J. Liu, Z. Wang, M. Zuba, Z. Peng, J.-H. Cui, and S. Zhou, "DA-sync: A Doppler-assisted time-synchronization scheme for mobile underwater sensor networks," *IEEE Trans. Mobile Comput.*, vol. 13, no. 3, pp. 582–595, Mar. 2014.

[8] F. Zhou, Q. Wang, D. Nie, and G. Qiao, "DE-sync: A Doppler-enhanced time synchronization for mobile underwater sensor networks," *Sensors*, vol. 18, no. 6, p. 1710, May 2018.

[9] F. Zhou, Q. Wang, G. Han, G. Qiao, Z. Sun, and A. Niaz, "APE-sync: An adaptive power efficient time synchronization for mobile underwater sensor networks," *IEEE Access*, vol. 7, pp. 52379–52389, 2019.

[10] Y. R. Faizulkhakov, "Time synchronization methods for wireless sensor networks: A survey," *Program. Comput. Softw.*, vol. 33, no. 4, pp. 214–226, Jul. 2007, doi: 10.1134/s0361768807040044.

[11] S. Mason, C. Berger, S. Zhou, and P. Willett, "Detection, synchronization, and Doppler scale estimation with multicarrier waveforms in underwater acoustic communication," *IEEE J. Sel. Areas Commun.*, vol. 26, no. 9, pp. 1638–1649, Dec. 2008.

[12] J. Liu, Z. Wang, Z. Peng, and M. Zuba, "TSMU: A time synchronization scheme for mobile underwater sensor networks," presented at the IEEE Global Telecommun. Conf., Dec. 2011, doi: 10.1109/GLOCOM.2011.6134447.

[13] O. Pallares, P.-J. Bouvet, and J. del Rio, "TS-MUWSN: Time synchronization for mobile underwater sensor networks," *IEEE J. Ocean. Eng.*, vol. 41, no. 4, pp. 763–775, Oct. 2016.

[14] C. Knapp and G. Carter, "The generalized correlation method for estimation of time delay," *IEEE Trans. Acoust., Speech, Signal Process.*, vol. ASSP-24, no. 4, pp. 320–327, Aug. 1976, doi: 10.1109/TASSP.1976.1162830.

[15] S. Ganeriwal, R. Kumar, and M. Srivastava, "Timing-sync protocol for sensor networks," presented at the Int. Conf. Embedded Netw. Sensor Syst., Nov. 2003, doi: 10.1145/958491.958508.
[16] R. Shams, P. Otero, M. Aamir, and F. H. Khan, "Joint algorithm for multi-hop localization and time synchronization in underwater sensors networks using single anchor," *IEEE Access*, vol. 9, pp. 27945–27958, 2021.
[17] C. Lv, "Research on V-time synchronization algorithm for underwater sensor networks based on energy clustering," *Modern Comput. Prof. Ed.*, vol. 620, no. 20, pp. 11–15, 2018.
[18] Y. Yao, G. Liu, and W. Kong, "Time synchronization algorithm for underwater sensors based on Doppler velocimetry," *Comput. Eng.*, vol. 47, no. 4, p. 6, 2021.
[19] C. Sun, F. Yang, and L. Ding, "Multi-hop time synchronization for underwater acoustic networks," *Oceans*, vol. 14, no. 1, pp. 65–80, 2012, doi: 10.1109/OCEANS.2012.6404923.
[20] H. Naman and A. Abdelkareem, "Multipath geometry channel model in shallow water acoustic communication," *J. Mar. Sci. Appl.*, vol. 22, no. 2, pp. 359–369, 2023, doi: 10.1007/s11804-023-00339-5.
[21] H. A. Naman and A. E. Abdelkareem, "Variable direction-based self-interference full-duplex channel model for underwater acoustic communication systems," *Int. J. Commun. Syst.*, vol. 35, no. 7, May 2022, Art. no. e5096. [Online]. Available: https://api.semanticscholar.org/CorpusID:246512495
[22] A. F. Rasheed and A. E. Abdelkareem, "Performance evaluation of MAC protocols with multi-sink for mobile UWSNs," *Int. J. Comput. Netw. Inf. Secur.*, vol. 11, no. 7, pp. 1–7, Jul. 2019, doi: 10.5815/ijcnis.2019.07.01.

SUN DAJUN received the B.S., M.S., and Ph.D. degrees in underwater acoustics engineering from Harbin Engineering University, Harbin, China, in 1999.

From 2001 to 2004, he was an Associate Professor and a Master's Supervisor with Harbin Engineering University, where he has been a Professor and a Doctoral Supervisor, since 2004. From 2003 to 2013 and from 2013 to 2016, he was the Vice Dean and the Dean of the School of Hydroacoustic Engineering, Harbin Engineering University, where he was the Director of the Key Laboratory of Underwater Acoustic Technology, from 2014 to 2016. He has presided over and completed more than 30 scientific research projects, including the National 863 Project, National Science and Technology Major Projects, National Defense Basic Research, National Natural Science Foundation of China, and the Ministry of Science and Technology's Russia Cooperation Special Project, with a total funding of over 90 million yuan. He has obtained 18 authorized patents, transferred two patents, authored one textbook, published more than 60 papers, and obtained more than ten software copyrights.

Prof. Dajun is currently an Expert of the Underwater Acoustic Group and the Navy's Pre Research Expert Group, the Director of the National Key Laboratory of Underwater Acoustic Technology and Chinese Acoustic Society, the Chairperson of Heilongjiang Acoustic Society, and an Academic Committee Member of the Key Laboratory of Underwater Acoustic Communication of the Ministry of Education and the National Defense Technology Innovation Laboratory of Acoustic Intelligence Guidance and Control of the Chinese Academy of Sciences. He serves as the Chairperson for the Technical Committee of IEEE COA2016, a member of the Technical Committee for IEEE Ocean2016, and an Editorial Board Member for the *Journal of Harbin Engineering University*. He has been awarded the title of a Young Expert with Outstanding Contributions to the National Defense Industry, Heilongjiang May Fourth Youth Medal, Heilongjiang Provincial Government Special Allowance, and has won one ministerial level first prize (ranked first) and two second prizes (ranked third and seventh).

OUYANG YUJIE received the B.S. degree in underwater acoustics engineering from Harbin Engineering University, Harbin, China, in 2017, where he is currently pursuing the Ph.D. degree in information and communication engineering.

He has published two articles and possessing two patents.

Mr. Yujie was awarded the Bronze Prize in the Seventh China International "Internet Plus" Undergraduate Innovation and Entrepreneurship Competition.

HAN YUNFENG received the B.S. and Ph.D. degrees in underwater acoustics engineering from Harbin Engineering University, Harbin, China, in 2016.

He has been an Associate Professor with Harbin Engineering University, since 2020. His research interests include underwater positioning and navigation and the establishment of marine geodetic position benchmarks technology. In the past five years, as the Project Leader, he has undertaken and participated in more than ten scientific research projects, including National Key Research and Development Plans, National Level Scientific and Technological Innovation Projects, Provincial and Ministerial Level Projects, and the National Natural Science Foundation of China. More than ten articles have been published and 12 invention patents have been authorized.

Prof. Yufeng has successively won one special prize of the Surveying and Mapping Science and Technology Award, one first prize of the National Marine Engineering Science and Technology Award, one silver award of China Patent Award, the top ten Scientific and Technological Progress in Chinese universities, in 2017, the top ten Scientific and Technological Progress in China's Oceans in 2015, and the National Marine Engineering Outstanding Contribution Award.